Agricultural and Forest Meteorology 249 (2018) 275–285

Contents lists available at ScienceDirect

Agricultural and Forest Meteorology

journal homepage: www.elsevier.com/locate/agrformet

NDVI derived from near-infrared-enabled digital cameras: Applicability across different plant functional types

Gianluca Filippa[a,*], Edoardo Cremonese[a], Mirco Migliavacca[b], Marta Galvagno[a], Oliver Sonnentag[c], Elyn Humphreys[d], Koen Hufkens[h], Youngryel Ryu[f], Joseph Verfaillie[g], Umberto Morra di Cella[a], Andrew D. Richardson[e]

[a] Environmental Protection Agency of Aosta Valley, ARPA Valle d'Aosta, Climate Change Unit, Italy
[b] Max Planck Institute for Biogeochemistry, Department Biogeochemical Integration, Jena, Germany
[c] Département de géographie & Centre d'études nordiques, Université de Montréal, Montréal, QC, Canada
[d] Department of Geography and Environmental Studies, Carleton University, Ottawa, ON, Canada
[e] Northern Arizona University School of Informatics Computing and Cyber Systems, Flagstaff, AZ, 86011, USA
[f] Department of Landscape Architecture and Rural Systems Engineering, Seoul National University, Republic of Korea
[g] Department of Environmental Science, Policy and Management, University of California, Berkeley, CA, USA
[h] Harvard University, Department of Organismic and Evolutionary Biology, Cambridge, MA, USA

ARTICLE INFO

Keywords:
Camera NDVI
Color indices
Near-surface remote sensing
PhenoCam
Phenology
Phenopix

ABSTRACT

Time series of vegetation indices (e.g. normalized difference vegetation index [NDVI]) and color indices (e.g. green chromatic coordinate [G_{CC}]) based on radiometric measurements are now available at different spatial and temporal scales ranging from weekly satellite observations to sub-hourly *in situ* measurements by means of near-surface remote sensing (e.g. spectral sensors or digital cameras). *In situ* measurements are essential for providing validation data for satellite-derived vegetation indices. In this study we used a recently developed method to calculate NDVI from near-infrared (NIR) enabled digital cameras ($NDVI_C$) at 17 sites (for a total of 74 year-sites) encompassing six plant functional types (PFT) from the PhenoCam network.

The seasonality of $NDVI_C$ was comparable to both NDVI measured by ground spectral sensors and by the moderate resolution imaging spectroradiometer (MODIS). We calculated site- and PFT-specific scaling factors to correct $NDVI_C$ values and recommend the use of site-specific NDVI from MODIS in order to scale $NDVI_C$. We also compared G_{CC} extracted from red-green-blue images to $NDVI_C$ and found PFT-dependent systematic differences in their seasonalities. During senescence, $NDVI_C$ lags behind G_{CC} in deciduous broad-leaf forests and grasslands, suggesting that G_{CC} is more sensitive to changes in leaf color and $NDVI_C$ is more sensitive to changes in leaf area. In evergreen forests, $NDVI_C$ peaks later than G_{CC} in spring, probably tracking the processes of shoot elongation and new needle formation. Both G_{CC} and $NDVI_C$ can be used as validation tools for the MODIS Land Cover Dynamics Product (MCD12Q2) for deciduous broad-leaf spring phenology, whereas $NDVI_C$ is more comparable than G_{CC} with autumn phenology derived from MODIS. For evergreen forests, we found a poor relationship between MCD12Q2 and camera-derived phenology, highlighting the need for more work to better characterize the seasonality of both canopy structure and leaf biochemistry in those ecosystems.

Our results demonstrate that $NDVI_C$ is in excellent agreement with NDVI obtained from spectral measurements, and that $NDVI_C$ and G_{CC} can complement each other in describing ecosystem phenology. Additionally, $NDVI_C$ allows the detection of structural changes in the canopy that cannot be detected by visible-wavelength imagery.

1. Introduction

Vegetation phenology (the study of the timing of recurrent biological events) is highly sensitive to climate variability and change (Rosenzweig et al., 2007; Migliavacca et al., 2012; Richardson et al., 2013). Phenological time-series based on radiometric measurements are now available, covering different spatial and temporal scales ranging from weekly satellite observations to sub-hourly *in situ* measurements by means of, e.g. spectral sensors or digital repeat photography. Regarding satellite-based data, the trade-off between spatial and temporal resolution represents a critical

* Corresponding author.
E-mail address: gian.filippa@gmail.com (G. Filippa).

https://doi.org/10.1016/j.agrformet.2017.11.003
Received 11 April 2017; Received in revised form 31 August 2017; Accepted 4 November 2017
Available online 10 November 2017
0168-1923/

Table 1
Study site locations along with PhenoCam and Fluxnet site IDs, plant functional types (PFT) and years of data analyzed. PFT are as follows: CRO, croplands; DBF, deciduous broad-leaf forests; ENF, evergreen needle-leaf forests; GRA, grasslands; SHB, shrublands. Note that PFT are defined according to the vegetation that characterizes the chosen regions-of-interest. They do not necessarily match the PFT classification for the whole site. Asterisks denote sites where light-emitting diode (LED) sensors were also available.

PhenoCam ID	Fluxnet ID	Coords (lat, long)	Years	PFT	Reference
southerngreatplains	US-ARM	36.7, −97.5	2012–2015	CRO	Fischer et al. (2007)
bartlett*	US-Bar	44.1, −71.3	2010–2015	DBF	Richardson et al. (2007)
harvardbarn2*	US-Ha1	42.5, −72.2	2012–2015	DBF/ENF	Magill et al. (2004)
willowcreek	US-WCr	45.8, −90.1	2012–2015	DBF	Cook et al. (2004)
freemanwood	US-FR3	29.9, −98.0	2012–2013	DBF	Heinsch et al. (2004)
alligatoriver	US-NC4	35.8, −75.9	2013–2015	DBF	www.fws.gov/refuge/Alligator_River/
turkeypointenf39	CA-TP4	42.7, −80.4	2012–2015	ENF	Arain and Restrepo-Coupe (2005)
oregonMP		44.5, −121.6	2012–2015	ENF	Thomas et al. (2009)
vaira*	US-Var	38.4, −121.0	2011–2015	GRA	Baldocchi et al. (2004)
lethbridge	CA-Let	49.7, −112.9	2011–2015	GRA	Flanagan et al. (2002)
tonzi*	US-Ton	38.4, −121.0	2011–2015	DBF/GRA	Baldocchi et al. (2004)
ibp		32.6, −106.8	2014–2015	GRA	Havstad et al. (2000)
canadaOBS	CA-Obs	54.0, −105.1	2011–2015	MF	Gower et al. (1997)
merbleue*	CA-Mer	45.4, −75.5	2012–2015	SHB	Sonnentag et al. (2007)
luckyhills	US-Whs	31.7, −110.1	2014–2015	SHB	Emmerich (2003)
jernort		32.6, −106.8	2014–2015	SHB	Emmerich (2003)
burnssagebrush	US-Bsg	43.5, −119.7	2012–2015	SHB	oregonstate.edu/dept/eoarc/

limitation especially in heterogeneous, fragmented ecosystems. To overcome this limitation, and in the attempt to fill the gap between point and landscape-level observations, the use of near-surface remote sensing has been notably growing in the last 20 years (Brown et al., 2016). In this context, digital repeat photography (e.g. Richardson et al., 2007, 2009; Sonnentag et al., 2012) is an attractive option because images can be analyzed either qualitatively or quantitatively (Kosmala et al., 2016), and analyses can focus on individual organisms or integrate across the field-of-view to obtain community- or canopy- or ecosystem-level phenological information.

The Normalized Difference Vegetation Index (NDVI, Tucker, 1979) has been widely used to monitor the timing and magnitude of the seasonal development of the vegetation and link them to environmental factors such as temperature, precipitation and photoperiod (Jolly et al., 2005). The majority of studies focused on satellite data to retrieve phenological signals at regional to global scales (Zhang et al., 2003), or on ground spectral sensors to link NDVI and other vegetation indices to *in situ* biotic and abiotic measurements (Soudani et al., 2014). The coherence in space and time between different NDVI sources (satellite vs near-surface remote sensing) has been explored in boreal and temperate deciduous broad-leaf forests (Liu et al., 2015; Hwang et al., 2014), evergreen forests (Jin and Eklundh, 2014), arid grasslands/savannas (Fensholt et al., 2006). Similarly, satellite vegetation indices have been also compared to camera-based color indices (Klosterman et al., 2014; Hufkens et al., 2012). The cross-scale comparisons between near- and far-remote sensing showed in general better coherence over deciduous than evergreen vegetation (Jin and Eklundh, 2014), and in greenup rather than senescence (Klosterman et al., 2014; Hufkens et al., 2012).

Few studies attempted the in situ comparison between NDVI and camera-based G_{CC} (but see Nasahara and Nagai, 2015). For example, Nagai et al. (2012) examined the relationship between NDVI or the enhanced vegetation index (EVI) and color indices in an evergreen forest in Japan demonstrating the ability of the latter to capture seasonal vegetation cycles. This comparison is often complicated by the different geometry (view angle and field-of-view dimension) of spectral sensors and digital cameras, especially in canopies with complex or multi-layered structures (Ryu et al., 2014; Migliavacca et al., 2011).

Recent developments in camera technology led to inexpensive, near-infrared (NIR) enabled security cameras, allowing the sequential capture of images covering visible-only and of combined visible and NIR images to calculate camera-based NDVI ($NDVI_C$, Petach et al., 2014). Results showed that the seasonal cycle of $NDVI_C$ is almost identical to that of NDVI measured using narrow-band spectral instruments, or retrieved from the moderate resolution imaging spectroradiometer (MODIS), demonstrating the potential of NIR-enabled cameras. The PhenoCam Network (http://phenocam.sr.unh.edu/webcam/) consists now of 340 sites equipped with networked digital cameras, of which two hundred are NIR-enabled cameras such as the ones used in Petach et al. (2014), thereby allowing to extend the analysis across multiple years and different plant functional types.

In the present paper, we analyzed a large dataset of visible plus NIR images across 17 North American sites encompassing six plant functional types (PFT) for a total of 74 year-sites of data from the PhenoCam image archive. Our objectives are:

(a) to compare $NDVI_C$ and G_{CC} seasonal trajectories across different PFT and identify potential differences in their phenology;
(b) to compare $NDVI_C$ and spectral measurements at different scales, including NDVI from MODIS and measured by ground light-emitting diodes (LED) sensors (Ryu et al., 2010);
(c) to examine the consistency between camera-derived phenological transition dates and the MODIS Land Cover Dynamics Product (MCD12Q2) with different methods for deciduous broad-leaf and evergreen needle-leaf forests.

2. Materials and methods

The seventeen sites included in this study belong to the PhenoCam network (http://phenocam.sr.unh.edu/webcam/) and are located in mid-latitude US and Canada (Table 1). The majority of them also belong to other observational networks such as Fluxnet (https://fluxnet.ornl.gov/). Each site is equipped with a NetCam SC IR security camera (StarDot Technologies, Buena Park, CA), featuring a Micron $\frac{1}{2}$" CMOS active-pixel digital imaging sensor and configured for 1.3 megapixel (1296 × 976) output. Camera channels are centered at 600, 530, 450 nm for red, green and blue, respectively (unpublished data). The camera was set at manual (fixed) white balance and automatic exposure. Five sites were also equipped with LED sensors. Peak sensitivities (and full width half maximum, FWHM) of LED sensors were at 646 (56) and 843 (72) nm, for red and NIR, respectively. These self-manufactured spectral sensors were first tested by Ryu et al. (2010) and have proven to be comparable to traditional radiometers.

Extraction of color and vegetation indices. Digital images were processed using the R package `phenopix` (Filippa et al., 2016). For each site one or more region-of-interest (ROI) was chosen, which restricts all subsequent analyses on that subset of pixels. ROIs can be viewed on the PhenoCam web page for each site (http://phenocam.sr.unh.edu/webcam/). RGB images were processed to obtain seasonal trajectories of green chromatic coordinates (G_{CC}, Gillespie et al., 1987). Camera

NDVI ($NDVI_C$) was computed based on simultaneous processing of sequentially-captured RGB and NIR + RGB images according to Petach et al. (2014). Briefly, $NDVI_C$ is calculated by extracting the red digital numbers (DN) from a RGB-image and the NIR DN from a NIR + RGB-image acquired few seconds apart. Both values are corrected for the exposure of the respective image prior to NDVI calculation.

G_{CC} time series were filtered with a combination of three filtering algorithms: (a) a threshold filter based on sun position excluding from the processing images acquired with a sun angle lower than 5° above the horizon; (b) a *spline* filter (Migliavacca et al., 2011) based on recursive spline smoothing and residual computation followed by removal of outliers falling outside an envelope of 5 times the standard deviation of the residuals; (c) a *max* filter following the method of Sonnentag et al. (2012), based on the identification of the 90th percentile values in a three-day moving window. $NDVI_C$ time series were subjected to similar filtering procedures, except that (b) was used with an envelope of 1.8 times the standard deviation of the residuals, an empirically-defined threshold based on residual distribution. We compared the *spline* filter to a more sophisticated method that finds the optimal span of a smoothing function (local polynomial regression, Cleveland, 1979) fitted through the data, based on Bayesian Information Criterion minimization (LOESS-BIC). In section SI1 we show that our empirical spline method results in phenological information comparable to the LOESS-BIC method. The empirical model is less computationally intense and therefore preferable for dealing with large databases.

Additionally, we took advantage of an existing snow classification for the PhenoCam image archive flagging each image with snow on canopy or ground (Richardson et al., in review). $NDVI_C$ appears particularly sensitive to the presence of snow cover, therefore data points with snow in the image were removed and replaced with a winter baseline value (SI2).

Scaling factors. Petach et al. (2014) showed that $NDVI_C$ raw values must be scaled in order to compare them to NDVI measurements obtained from spectral sensors (either *in situ* or remotely sensed). This step is needed because the spectral response of the CMOS sensor in the R, G, B and NIR of the Stardot camera is different compared to spectral measurements. We scaled $NDVI_C$ to the MODIS MCD43A2 product ($NDVI_M$). We extracted seasonal $NDVI_M$ trajectories on 3 × 3 pixel windows centered on each study site. The 9 pixels trajectories were first filtered with the MCD43A2 Bidirectional Reflectance Distribution Function (BRDF) Albedo Quality product. Scaling factors were computed by linear regression between the seasonal course of $NDVI_C$ and $NDVI_M$ following the formula:

$$NDVI_C = NDVI_M \cdot b + c \quad (1)$$

where b and c are the scaling factors. Because MCD43A2 is a 8-day product compositing 16 days of images, we used a data-driven approach (SI3) to establish the best matching between $NDVI_C$ and $NDVI_M$ data, i.e. a 10-day left-aligned moving average of $NDVI_C$.

Comparison of $NDVI_C$ with ground NDVI measurements. $NDVI_C$ was compared to NDVI measured by LED sensors ($NDVI_{LED}$, Ryu et al., 2010, 2014) at 5 sites: bartlett, vaira, tonzi, harvardbarn2 and merbleue. LED sensors are pointed nadir and have a field-of-view of 180°. $NDVI_{LED}$ is typically recorded every half hour. For this analysis we used daily-aggregated data, obtained by averaging values recorded in a two-hour interval around solar noon. For the five sites equipped with LED sensors, we also used $NDVI_{LED}$ to compute scaling factors.

Extraction of phenological dates from G_{CC}, $NDVI_C$ and comparison with MODIS Land Cover Dynamics Product (MCD12Q2). A double logistic function (Klosterman et al., 2014) was fitted to the seasonal trajectories of $NDVI_C$ and G_{CC}. Four different methods were then used to extract phenological transition dates on the fitted curves (namely *trs*, *derivatives*, *klosterman* and *gu* methods), described in detail in Filippa et al. (2016) and illustrated in Fig. SI4. All methods provide an estimation of uncertainty of the transition dates based on the resampling of the time series and extraction of the dates at each iteration (n = 500) as described in Filippa et al. (2016). From the uncertainty ensemble we calculated the median transition date and its mean absolute deviation (MAD).

The MCD12Q2 Land Cover Dynamics Product (spatial resolution 250 m) was obtained on 3 × 3 pixel windows centered on the study sites. For each scene and year four transition dates corresponding to Greenup, Maturity, Senescence and Dormancy were obtained, computed with a method similar to Klosterman et al. (2014). From the nine pixel values we calculated the median and the MAD. The relationship between MCD12Q2-derived and $NDVI_C$-derived dates was evaluated by means of linear regressions in a statistical framework that accounts also for uncertainty. Briefly, each regression analysis was replicated 500 times with observation points sampled (i) from the transition dates uncertainty ensemble, for $NDVI_C$-derived dates, and (ii) from a normally distributed population generated with the 9-pixel median and MAD values for $NDVI_M$-derived dates. This procedure generally results in poorer relationship scores compared to traditional linear regression, but allows for a more robust assessment of the uncertainty of the estimated transition dates. The coefficient of determination (r^2), root mean square error (RMSE) and model bias (BIAS) were computed for each of the 500 regressions and averaged.

3. Results

Seasonal trajectories of $NDVI_C$ and G_{CC} across different PFTs. Representative time series of G_{CC} and $NDVI_C$ for each PFT are show in Fig. 1 for 2013 and 2014. Deciduous broad-leaf forests are characterized by synchronous $NDVI_C$ and G_{CC} trajectories until the seasonal maximum of canopy development is reached. During the greendown period (Elmore et al., 2012), a small but consistent departure between G_{CC} and $NDVI_C$ occurs and gets amplified in autumn, when the decrease in $NDVI_C$ lags behind G_{CC} by several days.

Evergreen needle-leaf forests are characterized by an overall smaller seasonal amplitude in both G_{CC} and $NDVI_C$ compared to DBFs. The G_{CC} seasonal trajectory is roughly sinusoidal with a short baseline in winter. In contrast, $NDVI_C$ shows an abrupt increase around the beginning of July for both years. This lag in $NDVI_C$ with respect to G_{CC} is consistent across ENFs. We observed an earlier drop in $NDVI_C$ in autumn (beginning of October) as compared to G_{CC}, which also shows a decrease at that time, but smaller.

The seasonal trajectories of $NDVI_C$ and G_{CC} for burnssagebrush, a dry shrubland, show comparable seasonal dynamics, but differences in the year-to-year variability. In particular, G_{CC} peak is similar for 2013 and 2014, whereas $NDVI_C$ peak is remarkably lower in 2013 than in 2014. More generally, shrubland sites included in this study range from peatlands (merbleue) and dry (burnssagebrush) sites, to water limited sites (jernort and luckyhills), therefore patterns are not all consistent. However, the seasonality of $NDVI_C$ in SHBs is in general very similar to that of G_{CC}. The same is also true for the only cropland site included, i.e. southerngreatplains, even though in this PFT, inter-year variability in the behavior of G_{CC} and $NDVI_C$ is probably associated to different crops. Similar to DBFs, Lethbridge grassland site shows a lag in autumn phenology, with $NDVI_C$ reaching the autumn baseline about two weeks later than G_{CC}.

To evaluate the relationship between $NDVI_C$ and G_{CC} across all PFTs in terms of seasonal transition dates, we used the *gu* method on both indices. For this analysis, sites showing multiple seasonal peaks (i.e. croplands or water limited ecosystems, for which the double-logistic fitting offered poor results) were excluded. Results are shown in Fig. 2 for DBFs and GRAs, and Fig. 3 for ENFs. For DBFs and GRAs, upturn date (UD) occurs between day of year (DOY) 100 and 150 except for ibp, a dry grassland with a short seasonal cycle beginning slightly before DOY 200. Stabilization date (SD) and downturn date (DD) occur over a longer time frame (DOY 110–220 and 200–300, respectively). Recession date (RD) across DBFs and GRAs spans roughly 50 days (DOY

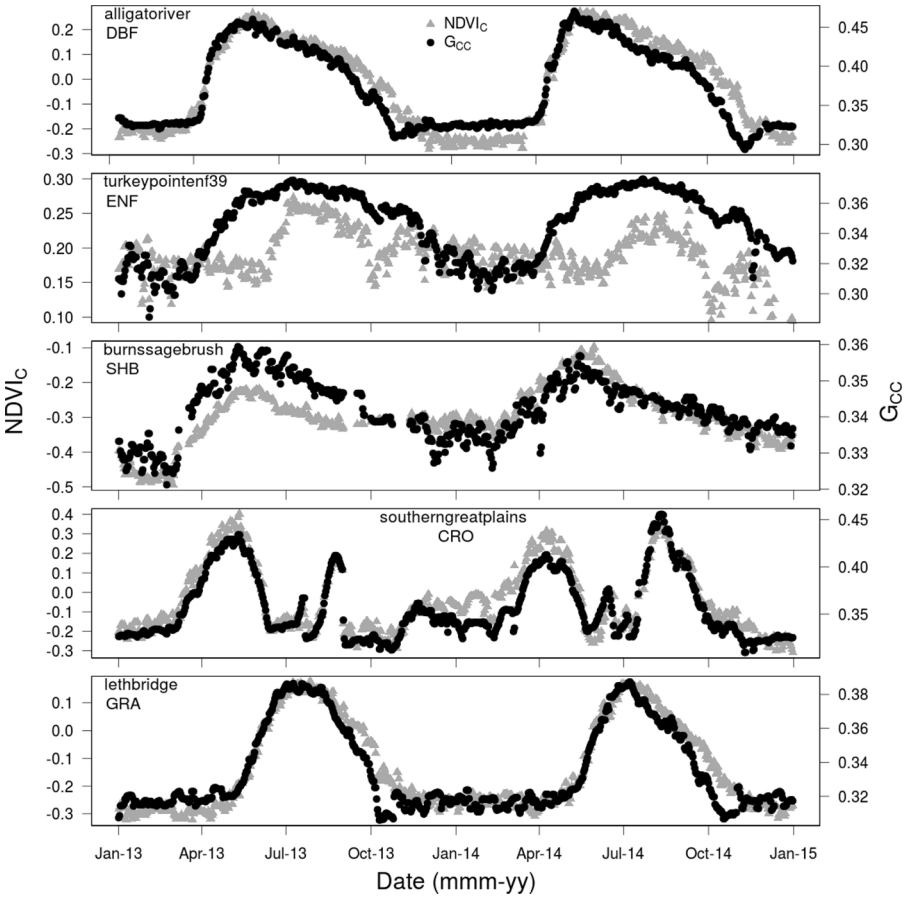

Fig. 1. Two-year of daily $NDVI_C$ and G_{CC} from a selection of sites included in this study. DBF: deciduous broad-leaf forest; ENF: evergreen needle-leaf forest; SHB: shrubland; CRO: cropland; GRA: grassland.

250–300) for G_{CC} and 100 days (DOY 250–350) for $NDVI_C$. The greening dates (UD and SD) extracted from G_{CC} and $NDVI_C$ are highly correlated and close to the 1:1 line, with an RMSE of about 4–6 days and a bias of about one week. DD is the transition date showing the largest error in the single dates and lower r^2 in the relationship. The regression statistics of RD demonstrate a poorer relationship than for spring, but interestingly show a 19-day positive bias (i.e. $NDVI_C$ transition dates occurring later than G_{CC}), thereby allowing to generalize the autumn lag between G_{CC} and $NDVI_C$ decrease across GRA and DBF functional types.

Unlike DBFs and GRAs, the methods based on derivatives (i.e. all except *trs* method) did not give satisfactory results for ENFs. The much lower signal-to-noise ratio in the time series of both $NDVI_C$ and G_{CC} resulted in poor performance of the double-logistic fittings and higher uncertainty in the estimated dates. Instead, the method chosen for ENFs was based on reaching 40% of the amplitude of the seasonal trajectory. Compared to DBFs and GRAs, transition dates for ENFs (Fig. 3) are less consistent between $NDVI_C$ and G_{CC}. A positive bias (29 days) in the start of season (sos) was found, indicating that for all ENF sites $NDVI_C$ starts increasing later by about 1 month compared to G_{CC}. The DOY of peak production (pop) occurs on average 13 days later for $NDVI_C$ than for G_{CC}, whereas the opposite is true in autumn, with a negative bias (22 days) in end of season (eos).

Comparison of $NDVI_C$ with MODIS seasonal trajectories and scaling

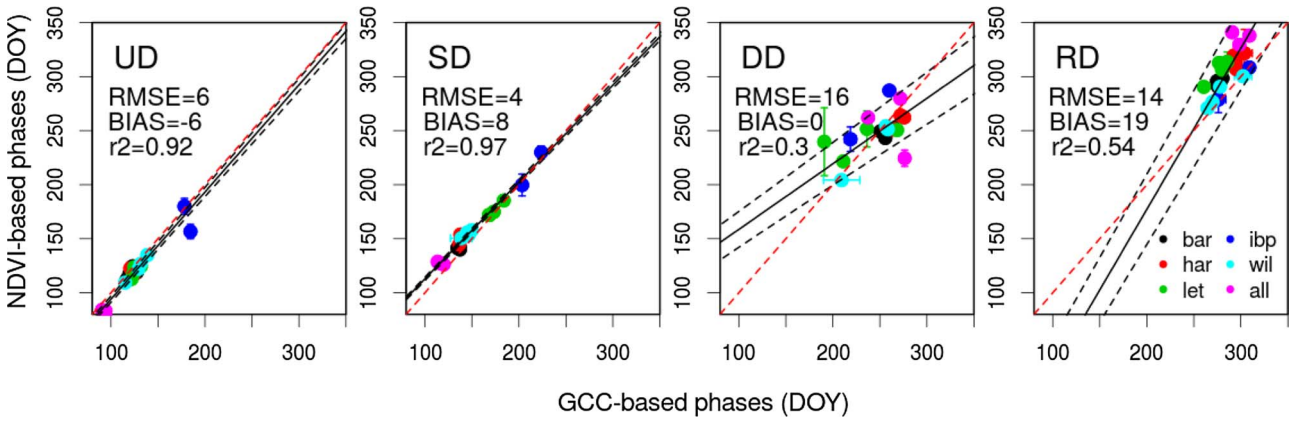

Fig. 2. Relationship between transition dates extracted from G_{CC} (*x*-axis) and $NDVI_C$ (*y*-axis) time series for deciduous broad-leaf forests (DBF) and grasslands (GRA). Each data point is a site-year median date. Error bars represent the MAD. The red dashed line is the 1:1, whereas black lines represent the linear fit (solid) and its uncertainty (dashed). Site abbreviations: bar: bartlett; har: harvardbarn2; let: lethbridge; ibp: ibp; wil: willowcreek; all: alligatorriver. Abbreviations: UD: upturn date; SD: stabilization date; DD: downturn date; RD: recession date. (For interpretation of the references to color in this figure legend, the reader is referred to the web version of this article.)

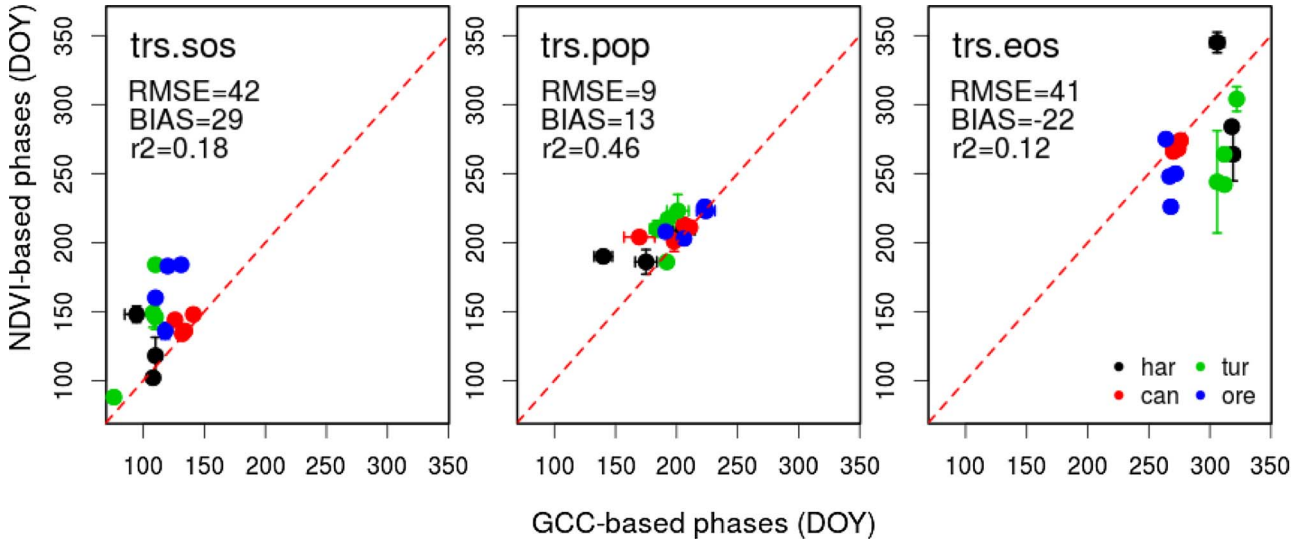

Fig. 3. Relationship between transition dates extracted from G_{CC} (*x*-axis) and NDVI$_C$ (*y*-axis) for ENFs. The extraction method used here is a fixed 40% threshold (*trs*). Each point is a site-year median transition date. Error bars represent the MAD. The red dashed line is the 1:1. Site abbreviations: har: harvardbarn2; tur: turkeypointenf39; can: canadaOBS; ore: oregonMP. Abbreviations: trs.sos: threshold-based start of season; trs.pop: doy of peak of production; trs.eos: threshold-based end of season. (For interpretation of the references to color in this figure legend, the reader is referred to the web version of this article.)

Table 2
Site-specific and PFT-specific scaling factors computed as regression coefficients of the linear relationship between NDVI$_M$ and NDVI$_C$ for each site included in this study. PFT-specific scaling factors are computed regressing all site data of a given PFT together. Lines in *italics* report scaling factors computed between NDVI$_{LED}$ and NDVI$_C$. n = number of observations for each regression. All regressions are statistically significant ($p < 0.01$), except for oregonMP.

Site-specific	PFT	Slope (b)	Intercept (c)	r^2	n
southerngreatplains	CRO	0.3 ± 0.33	0.42 ± 0.01	0.12	102
alligatoriver	DBF	0.47 ± 0.070	0.7 ± 0.00	0.88	109
bartlett	DBF	0.55 ± 0.06	0.71 ± 0.00	0.86	191
bartlett (LED)		*0.83 ± 0.02*	*0.60 ± 0.00*	*0.79*	*662*
freemanwood	DBF	0.49 ± 0.44	0.54 ± 0.07	0.40	35
harvardbarn2	DBF	0.61 ± 0.09	0.76 ± 0.01	0.84	141
harvardbarn2 (LED)		*0.56 ± 0.01*	*0.75 ± 0.00*	*0.82*	*1208*
willowcreek	DBF	0.78 ± 0.1	0.66 ± 0.00	0.90	100
oregonMP	ENF	45.29 ± -38.07	-9.38 ± -8.46	0.00	152
turkeypointenf39	ENF	5.94 ± 3.12	-0.47 ± 0.6	0.41	96
ibp	GRA	1.25 ± 0.38	0.54 ± 0.1	0.72	69
lethbridge	GRA	0.80 ± 0.14	0.44 ± 0.02	0.79	127
tonzi	GRA	0.60 ± 0.19	0.63 ± 0.06	0.52	148
tonzi (LED)		*0.97 ± 0.02*	*0.58 ± 0.00*	*0.82*	*375*
vaira	GRA	0.66 ± 0.17	0.62 ± 0.05	0.63	137
vaira (LED)		*1.06 ± 0.01*	*0.63 ± 0.00*	*0.88*	*1274*
canadaOBS	MF	2.48 ± 1.07	0.56 ± 0.00	0.44	116
burnssagebrush	SHB	1.66 ± 0.90	0.64 ± 0.25	0.35	108
jernort	SHB	0.19 ± 0.09	0.22 ± 0.02	0.57	63
luckyhills	SHB	0.44 ± 0.64	0.36 ± 0.22	0.22	33
merbleue	SHB	1.88 ± 0.54	0.67 ± 0.00	0.72	80
merbleue (LED)		*1.38 ± 0.01*	*0.65 ± 0.00*	*0.92*	*965*
PFT-specific	DBF	0.57 ± 0.06	0.70 ± 0.00	0.72	576
	ENF	1.70 ± 0.56	0.47 ± 0.05	0.41	212
	GRA	0.59 ± 0.21	0.52 ± 0.05	0.20	481
	SHB	1.83 ± 0.17	0.67 ± 0.03	0.88	251
Petach et al. (2014)	DBF	0.53 ± 0.02	0.84 ± 0.01	0.89	

factors. NDVI$_C$ was compared with NDVI$_M$ seasonal trajectories in order to define appropriate scaling factors for NDVI$_C$ (Petach et al., 2014). First, for each site NDVI$_M$ was regressed against 10-day left-aligned running medians of NDVI$_C$ values (SI3). DBFs and GRAs show consistently tight relationships, whereas ENFs, SHBs, and CROs do not (Table 2). Therefore, for the estimation of PFT-specific scaling factors, we included only sites where the site-specific relationship was higher than 0.3, i.e. 14 out of 17 sites. On this subset we calculated the PFT-specific scaling factors. These PFT-specific scaling factors are then applied to the raw NDVI$_C$ data (Fig. 4). For DBFs, there is an excellent agreement between scaled NDVI$_C$ and NDVI$_M$, independently on whether NDVI$_C$ is scaled according to PFT-specific (grey triangles) or site-specific (black triangles) factors. For ENFs, the relationship between NDVI$_M$ and NDVI$_C$ is in general poor with tighter relationships for NDVI$_C$ scaled according to the site-specific scaling factor compared to the PFT-specific ones. In burnssagebrush, PFT-specific and site-specific scaled NDVI$_C$ are very close to each other. In contrast NDVI$_M$ shows a lower seasonal amplitude and temporal mismatch with NDVI$_C$, with earlier seasonal peaks in all three years included in the comparison. In lethbridge the site-scaled NDVI$_C$ is in good agreement with NDVI$_M$, whereas the PFT-scaling reduces the seasonal amplitude of NDVI$_C$. Spatial heterogeneity may be responsible for the temporal mismatch between NDVI$_C$ and NDVI$_M$ in southerngreatplains seasonal trajectories, however the PFT-specific scaling factor (extended from GRA) seems to better reproduce the amplitude of NDVI$_M$ signal compared to the site-specific factors. Scaling factors computed against data from LED sensors are different compared to those obtained from NDVI$_M$ at the same site, except for harvardbarn2 and merbleue (Table 2).

Comparison of in situ measurements: NDVI$_{LED}$ and NDVI$_C$. Fig. 5 shows a three-year time series comparing NDVI$_{LED}$ and NDVI$_C$. Overall, the seasonalities of NDVI$_C$ and NDVI$_{LED}$ are in excellent agreement. In DBF, the two sensors provide consistent seasonal NDVI trajectories both in terms of timing and magnitude. At bartlett, NDVI$_{LED}$ appears to be more affected by the presence of snow compared to NDVI$_C$. At vaira, the magnitude of NDVI$_C$ is lower than that of NDVI$_{LED}$, but the timing is similar across the three years. At tonzi and merbleue, both the magnitude and seasonality of NDVI$_{LED}$ and NDVI$_C$ are consistent.

MODIS Land Cover Dynamics Product (MCD12Q2) and NDVI$_C$. To compare our NDVI$_C$ measurements to satellite products, we regressed transition dates extracted from both G_{CC} and NDVI$_C$ time series against the corresponding estimates obtained from the MODIS Land Cover Dynamics Product (MCD12Q2). In order to exclude sites displaying multiple peaks during the season (e.g. southerngreatplains), and sites with very high spatial heterogeneity within the MODIS pixel (e.g. tonzi and vaira), the analysis was limited to DBFs and ENFs, and to spring (*UD*, *Greenup*, *sos*) and fall (*RD*, *Dormancy*, *eos*) transition dates. This analysis also tested four different methods of transition date extraction available in the `phenopix` R package (Fig. 6).

For DBFs, spring dates shows RMSEs of about 7 days with no substantial difference across methods and between G_{CC}- and NDVI$_C$-derived

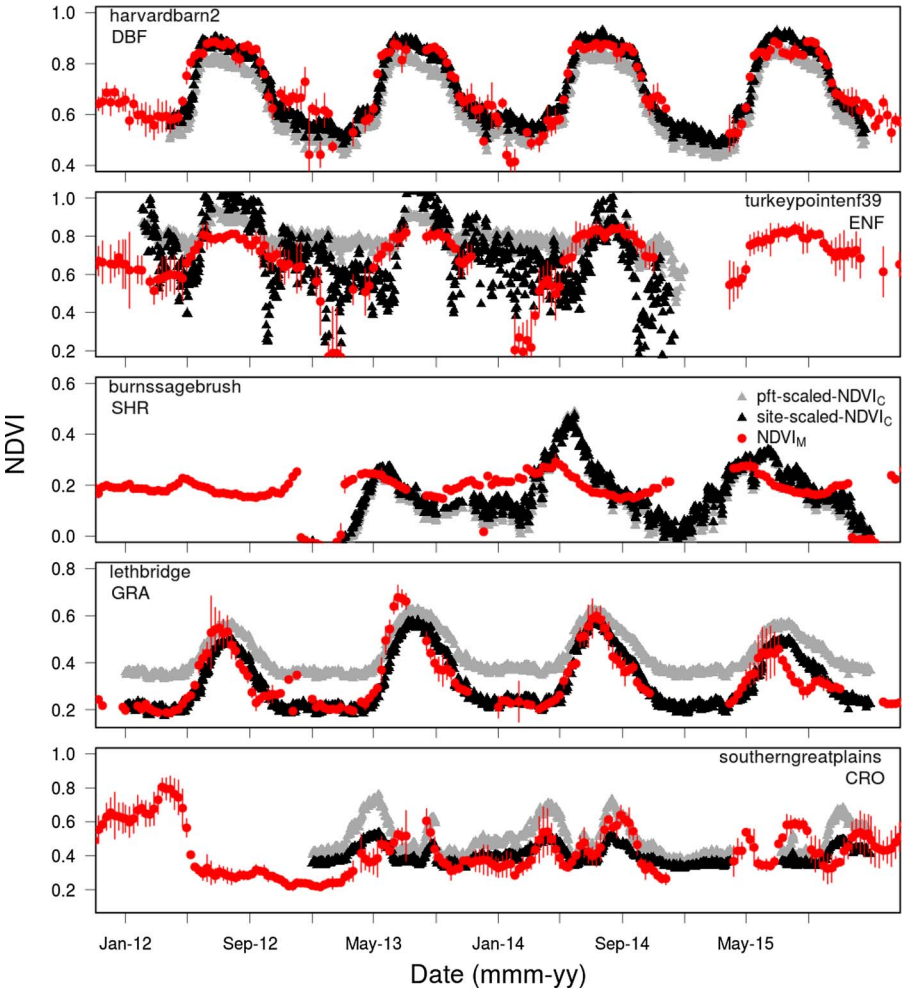

Fig. 4. A four-year (2012–2015) comparison between daily $NDVI_C$ and 8-day $NDVI_M$ for a selection of sites (Table 1. $NDVI_C$ absolute values are scaled according to the scaling factors reported in Table 2 (black triangles). Grey triangles are for $NDVI_C$ scaled with the PFT-specific scaling factors. For southerngreatplains we used the scaling factors calculated for GRAs. Error bars on $NDVI_M$ data represent the MAD on the 3 × 3 pixels window. (For interpretation of the references to color in this figure legend, the reader is referred to the web version of this article.).

transition dates. Consistently negative BIAS scores suggest earlier MODIS dates compared to either G_{CC} and $NDVI_C$, but with considerably lower values when dates are extracted with *gu* and *klosterman* methods. The r^2 of the relationships indicate an explained variance higher than 65% for greenup, being lower for the *derivatives* method compared to others. For autumn dormancy of DBFs, the best relationship is provided by the *gu* method applied to NDVI time series, with RMSE = 10 days, bias = 4 days and $r^2 > 0.7$.

Compared to DBFs, the relationship between MODIS- and phenocamera-derived transition dates at ENF sites was generally worse. For spring, the best result is achieved by the *klosterman* method applied to NDVI ($r^2 = 0.23$, RMSE = 13, bias = −26). Noteworthy is the fact that we found opposite signs for BIAS for $NDVI_C$ and G_{CC}, with $NDVI_C$ resulting in later greenup compared to MODIS and the opposite for G_{CC}. For dormancy, the *derivatives* approach applied to G_{CC} time series provides the best scores ($r^2 = 0.26$, RMSE = 28, BIAS = −6).

4. Discussion

4.1. Robustness of $NDVI_C$ measurements

This study provides the first analysis of a large dataset (74 site-years) of visible and visible + NIR images for the computation of paired G_{CC} and $NDVI_C$ using an image archive acquired by NIR-enabled digital cameras. After the pioneering work of Petach et al. (2014), several questions remained open. Does the relationship between $NDVI_C$ and spectral measurements verified on a single year above a deciduous canopy hold across multiple sites and PFTs? Can the proposed scaling factors – calculated for a deciduous canopy – be generalized across sites and, potentially, PFTs?

As for the first question, Fig. 5 demonstrates excellent agreement between $NDVI_{LED}$ and $NDVI_C$ across five different sites and four PFTs. These results indicate that the seasonal trajectory of $NDVI_C$ mirrors that of NDVI measurements obtained from spectral sensors across a range of ecosystems, even those characterized by a different canopy cover fraction (as for example at tonzi, a savanna with mixed grassland and deciduous trees). At Bartlett, the $NDVI_{LED}$ signal seems to deteriorate in winter likely because of snow on the ground, a less relevant problem for $NDVI_C$ because the analyzed ROI is specifically tailored on the tree crowns, therefore avoiding the integration of bare soil, whereas the nadir view of the LED sensors is more affected by background spectroscopic properties. This advantage of digital images over spectral measurements could be fully exploited in evergreen forests, where the presence of snow on trees often causes very noisy NDVI signals. Unfortunately the lack of radiometric NDVI measurements with a similar view angle compared to digital image acquisition prevents us from further exploring this hypothesis and future work should be oriented in this direction.

As for the second question, our data demonstrate that scaling factors may have great variation across sites (Table 2). This may be due to several reasons: (a) the different view angle of phenocameras and satellite data, (b) the different bands used for NDVI calculation in $NDVI_M$ and $NDVI_C$ (Hufkens et al., 2012), (c) a spatial mismatch between MODIS and phenocameras especially in fragmented landscapes, because the ROI of the cameras is specifically tailored on the canopies. In fact at two sites with low fractional cover (tonzi and vaira) scaling

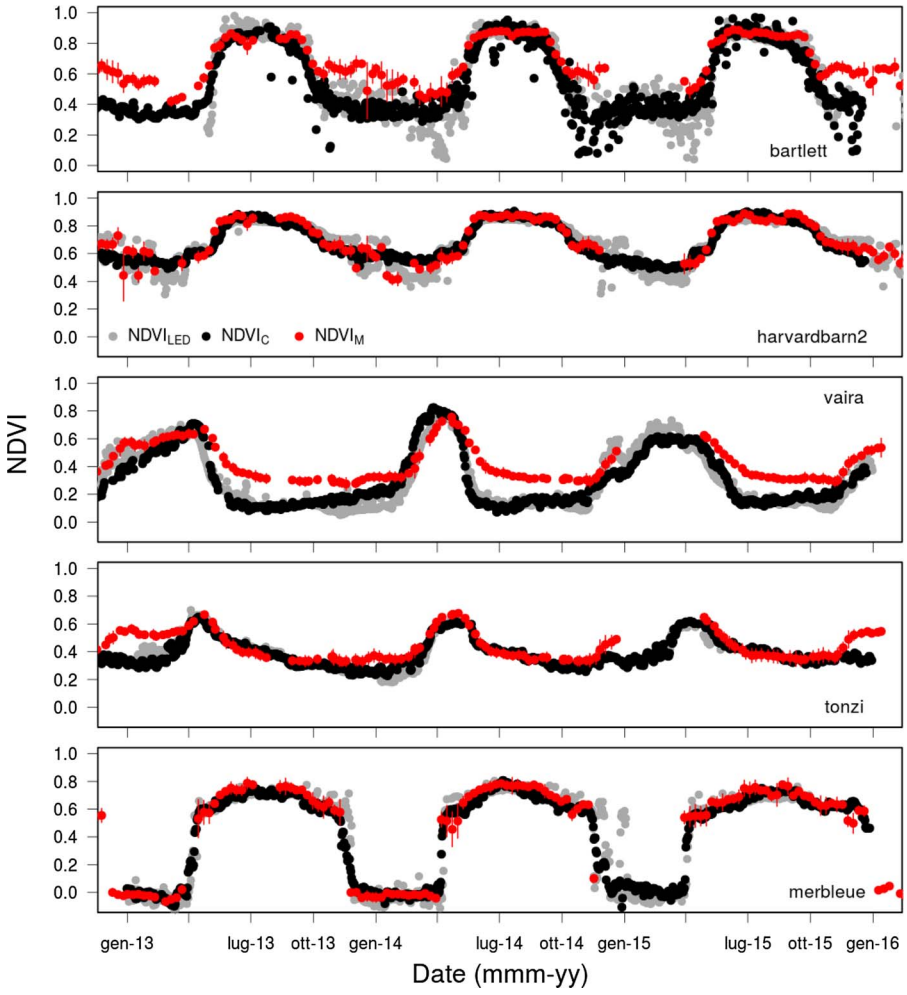

Fig. 5. Time series of NDVI$_{LED}$, NDVI$_M$ and scaled NDVI$_C$. The coefficients of determination of the relationship between NDVI$_C$ and NDVI$_{LED}$ are 0.79, 0.82, 0.88, 0.82 and 0.92 for bartlett, harvardbarn2, vaira, tonzi and merbleue, respectively. (For interpretation of the references to color in this figure legend, the reader is referred to the web version of this article.)

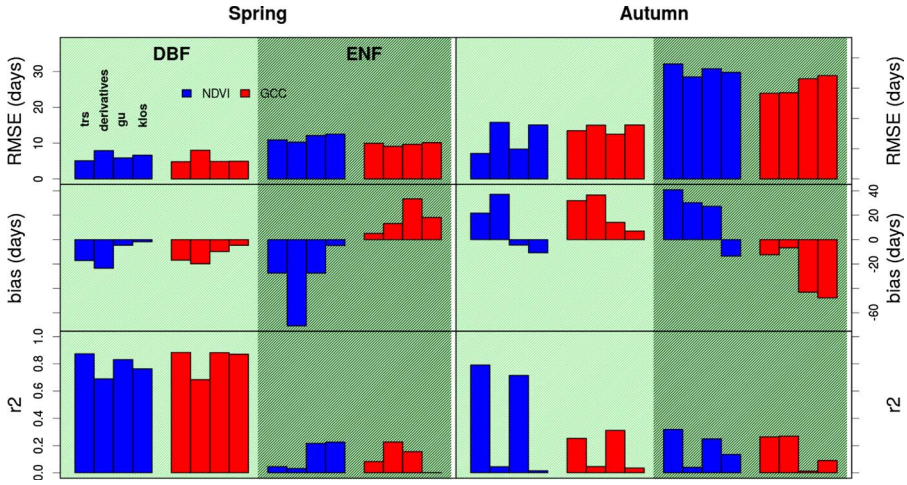

Fig. 6. Scores (i.e. root mean square error (RMSE), bias and r^2) of the linear relationships between near surface phenology (NDVI$_C$ and G_{CC}) and MODIS Land Cover Dynamics Product (MCD12Q2). Scores are shown for four different methods for the extraction of transition date (*trs*, *derivatives*, *klosterman* and *gu*, the four bars in the same subplot), separately for DBFs and ENFs (light and dark green backgrounds, respectively), and for NDVI$_C$-based and G_{CC} based phenology (blue and red bars, respectively). Spring transition dates are featured to the left, whereas autumn dates to the right. (For interpretation of the references to color in this figure legend, the reader is referred to the web version of this article.).

factors computed against ground LED sensors show better relationship than with MODIS, whereas at merbleue, where the vegetation cover is homogeneous and LED, cameras and satellite likely observe similar targets, scaling factors are more similar. This supports the hypothesis that spatial mismatch plays a role in the variability of scaling factors. Overall, scaling factors for DBFs are the most consistent, and they approach the values reported by Petach et al. (2014) (see Table 2).

We recommend the use of site-specific NDVI$_M$ data to scale NDVI$_C$ values. In the case that the MODIS pixel is not representative of the vegetation targeted by the cameras (which can be checked by visually comparing the seasonal trajectories), NDVI$_C$ should be scaled with ground spectral NDVI data, if available. Otherwise, PFT-specific scaling factors reported in Table 2 can be used for DBFs. For other PFTs, scaling factors computed in this study should be used with caution.

4.2. The seasonality of NDVI$_C$ and G_{CC}

The seasonal trajectory of NDVI$_C$ and G_{CC} shows remarkable differences (Fig. 1) which result in different transition dates (Figs. 2 and 3), and these differences are PFT-specific. Autumn decrease occurs

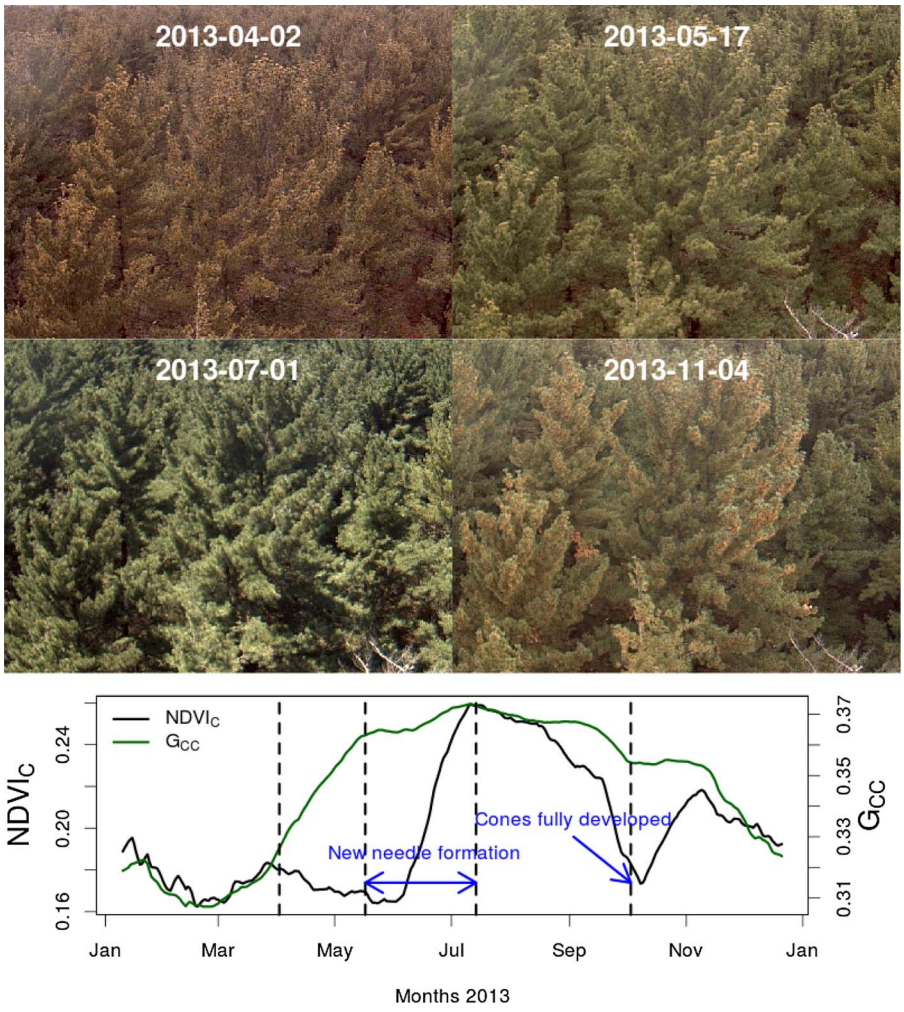

Fig. 7. Seasonal course of 20-days-moving-average G_{CC} and $NDVI_C$ values at TurkeyPointenf39 in 2013, along with selected photographs. Vertical lines in the time series correspond to the dates when the above pictures were taken. Phenological information (in blue) is obtained from aggregated phenological data collected in 2013 for about 300 Eastern White Pine individuals located in the Eastern US areas (data not shown, National Phenology Network, 2017). (For interpretation of the references to color in this figure legend, the reader is referred to the web version of this article.).

somewhat slower for $NDVI_C$ than for G_{CC} in DBFs and GRAs, resulting in a later start of dormancy of $NDVI_C$ compared to G_{CC}. This suggests that G_{CC} is more sensitive to slight changes in leaf colors in summer and pronounced leaf color change during senescence compared to $NDVI_C$, which in turn is more indicative of the leaf abscission and shedding processes during the senescence period. These findings agree with Keenan et al. (2014), who reported that declines in autumn leaf area index lagged declines in autumn G_{CC}, reflecting changing leaf color before actual leaf abscission in a temperate DBF.

The autumn lag is apparent also for temperate grasslands. A study combining phenocams and radiative transfer modelling in a Mediterranean grassland suggests that the lag between $NDVI_C$ and G_{CC} in the senescence period (dry-down in summer) is the result of different sensitivity of G_{CC} to the amount of senescent material in the canopy (ratio of dry/green biomass) and leaf area index compared to $NDVI_C$. G_{CC} is shown to be more sensitive to the dry/green biomass than $NDVI_C$, while $NDVI_C$ responds more to variation of LAI in the range between 1 and 3 m^2/m^2 (Luo et al., in review). In terms of transition dates, different temporal dynamics of $NDVI_C$ and G_{CC} result in a 20-day lag in the end of season (recession date, RD in Fig. 2) for DBFs and GRAs. This might have important implications when these data streams are used to constrain or to develop phenology models.

ENFs are characterized by a lower seasonal amplitude in both $NDVI_C$ and G_{CC}, and a lower signal-to-noise ratio, preventing us from using derivative-based extraction methods. Our results suggest that in such ecosystems, the most robust method for transition date computation is threshold-based (Fig. 3). With the *trs* method we were able to identify a generalized later spring increase in $NDVI_C$ compared to G_{CC} quantified at 29 days across all ENFs (Fig. 3).

An hypothesis for the asynchronous spring ramp in G_{CC} and $NDVI_C$ is the increase in foliar biomass associated with shoot elongation (Wingate et al., 2015) and the formation of new needles (Ryu et al., 2014), with no substantial change in the canopy greenness. In Fig. 7 we show the smoothed time course of G_{CC} and $NDVI_C$, along with representative photographs at turkeypointenf39 in 2013. The evergreen canopy (eastern white pine, *Pinus strobus*) turns from brownish in early April to green in May. This transition is characterized by a sharp increase in G_{CC}, while $NDVI_C$ remains low and rather constant. The following period is characterized by only slight increase in G_{CC} and a sharp $NDVI_C$ ramp. This period corresponds to the new needle formation; in *Pinus strobus* new needles emerge in the third decade of May and young needles tend to be completely formed at the end of June (National Phenology Network, 2017). Our data suggests therefore that while the level of green is already close to the maximum in spring, $NDVI_C$ tracks foliar biomass increase associated to new needle formation. The decrease in $NDVI_C$ in September corresponds to the ripening period of seed cones which turn from green to red, and are fully developed in early October (National Phenology Network, 2017). The significant presence of red cones may cause the observed decline in $NDVI_C$. Afterwards, cones begin dropping, resulting in green canopy dominating again the region-of-interest and producing a slight increase in $NDVI_C$ in November, before the onset of winter. This comparison with ground phenology suggests that in boreal and temperate ENFs, $NDVI_C$ allows the detection of structural changes in the canopy that cannot be detected by G_{CC}.

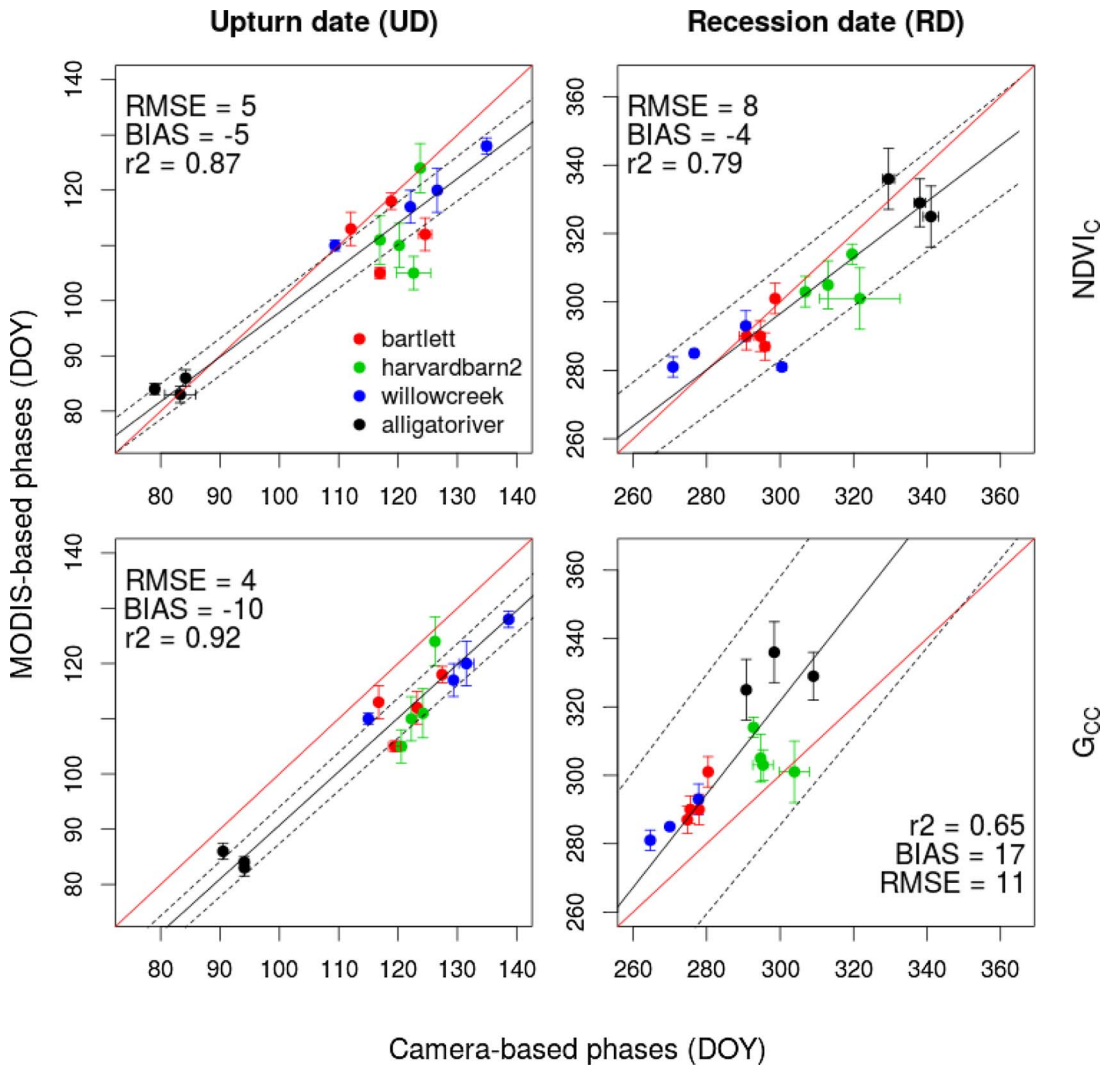

Fig. 8. Comparison of transition dates extracted from $NDVI_C$ using the *gu* method with the MODIS Land Cover Dynamics product (MCD12Q2) for deciduous broad-leaf forests (n = 15 site-years).

4.3. Comparison of camera-derived metrics and the MODIS Land Cover Dynamics Product (MCD12Q2)

Phenocamera networks provide invaluable ground data for the validation of phenology satellite products. Our analysis suggests that both G_{CC} and $NDVI_C$ can be used as validation tools for MCD12Q2 for DBF spring phenology, provided that transition dates are extracted with the *gu* or *klosterman* methods. Spring greenup is detected earlier by MODIS by about one week compared to both $NDVI_C$ and G_{CC}. This is likely because the oblique view of the camera solely tracks tree phenology whereas the nadir satellite view is more affected by the earlier greenup of the understory (Ryu et al., 2014). For autumn phenology, $NDVI_C$-dates extracted with the *gu* method perform better than other methods, and better than G_{CC}. A previous study comparing G_{CC} transition dates and MCD12Q2 across North American DBF showed a consistent bias for dormancy, with dates predicted from G_{CC} occurring 12 days earlier than those predicted from MCD12Q2 (Klosterman et al., 2014). In our study, the positive BIAS between G_{CC}-derived and MODIS-derived dates is even higher (17 days), whereas by using $NDVI_C$-derived dates not only we obtain a better relationship than for G_{CC}, but also an opposite and reduced BIAS (-4 days, Fig. 8).

Our study confirms better coherence in spring rather than in autumn DBF phenology. Hufkens et al. (2012) argued that more uncertain senescence dates are due to the fact that the rate of change in any vegetation index is more gradual in autumn. Furthermore, while greenup tends to be more homogeneous in space, higher heterogeneity in the canopy exists during senescence (Klosterman et al., 2014). This is likely the cause of higher uncertainty in MODIS-derived than in camera-derived dates (Fig. 8, right column). The discrepancy between camera- and satellite-derived senescence dates can also be associated to different degrees of deciduous or mixed canopy cover, with lower bias with increasing degree of deciduous species over evergreens (Klosterman et al., 2014).

For ENFs, the poor relationship between MCD12Q2 and camera-derived transition dates suggest the we are not yet able to properly describe the phenology of such ecosystems by means of currently available vegetation and color indices (Jönsson et al., 2010). One of the main problems in detecting evergreen phenology at high latitude from satellite is the small amplitude in the greenness signal combined with the presence of snow cover (Delbart et al., 2005). This was the case for all evergreen sites included in this study. Encouraging is the fact that the phenocamera approach can overcome the problem of background by properly choosing the region-of-interest of the analysis. Additionally, a growing body of research is currently addressing new vegetation indices including the clorophyill/carotenoid index (CCI, Gamon et al., 2016), the green/red vegetation index (GRVI, Nasahara and Nagai, 2015), particularly suitable for describing evergreen phenology, representing promising candidates for comparison with

vegetation indices such as $NDVI_C$.

5. Conclusion

In this work we demonstrate that $NDVI_C$ measurements derived from NIR-enabled digital cameras are robust and comparable to NDVI measured by ground spectral sensors ($NDVI_{LED}$) or satellite (MODIS) NDVI measurements. We show that scaling factors have to be applied to $NDVI_C$ in order to scale it to spectral NDVI measurements. Moreover, we demonstrate that simultaneous $NDVI_C$ and G_{CC} time series provide complementary phenological information by tracking different canopy-level processes, with potentially important implications for phenology models. We furthermore illustrate to what extent and how $NDVI_C$ and G_{CC} can be used as ground validation for the MODIS Land Cover Dynamics Product.

In the future, satellite imagery (eg. with the recently launched Sentinel suite) will provide 5-days, 10 m resolution remotely sensed data less prone to spatial and temporal mismatch, likely improving the relationship between near- and far-remote sensing, especially in ecosystems, such as evergreen forests, where this relationship is currently poor.

Acknowledgements

The development of PhenoCam has been supported by the Northeastern States Research Cooperative, NSF's Macrosystems Biology program (award EF-1065029 and EF-1702697), DOE's Regional and Global Climate Modeling program (award DE-SC0016011), and the US National Park Service Inventory and Monitoring Program and the USA National Phenology Network (grant number G10AP00129 from the United States Geological Survey). We acknowledge additional support, through the National Science Foundation's LTER program, for research at Harvard Forest (DEB-1237491), and Bartlett Experimental Forest (DEB-1114804). The National Research Foundation of Korea (NRF) supported making LED sensors (NRF-2011-0030485).

Appendix A. Supplementary data

Supplementary data associated with this article can be found, in the online version, at http://dx.doi.org/10.1016/j.agrformet.2017.11.003.

References

Arain, M.A., Restrepo-Coupe, N., 2005. Net ecosystem production in a temperate pine plantation in southeastern Canada. Agric. Forest Meteorol. 128, 223–241.
Baldocchi, D.D., Xu, L., Kiang, N., 2004. How plant functional-type, weather, seasonal drought, and soil physical properties alter water and energy fluxes of an oak-grass savanna and an annual grassland. Agric. Forest Meteorol. 123, 13–39.
Brown, T.B., Hultine, K.R., Steltzer, H., Denny, E.G., Denslow, M.W., Granados, J., Henderson, S., Moore, D., Nagai, S., SanClements, M., Sánchez-Azofeifa, A., Sonnentag, O., Tazik, D., Richardson, A.D., 2016. Using phenocams to monitor our changing earth: toward a global phenocam network. Front. Ecol. Environ. 14, 84–93.
Cleveland, W.S., 1979. Robust locally weighted regression and smoothing scatterplots. J. Am. Stat. Assoc. 74, 829–836.
Cook, B.D., Davis, K.J., Wang, W., Desai, A., Berger, B.W., Teclaw, R.M., Martin, J.G., Bolstad, P.V., Bakwin, P.S., Yi, C., Heilman, W., 2004. Carbon exchange and venting anomalies in an upland deciduous forest in northern Wisconsin, USA. Agric. Forest Meteorol. 126, 271–295.
Delbart, N., Kergoat, L., Toan, T.L., Lhermitte, J., Picard, G., 2005. Determination of phenological dates in boreal regions using normalized difference water index. Rem. Sens. Environ. 97, 26–38.
Elmore, A.J., Guinn, S.M., Minsley, B.J., Richardson, A.D., 2012. Landscape controls on the timing of spring, autumn, and growing season length in mid-Atlantic forests. Glob. Change Biol. 18, 656–674.
Emmerich, W.E., 2003. Carbon dioxide fluxes in a semiarid environment with high carbonate soils. Agric. Forest Meteorol. 116, 91–102.
Fensholt, R., Sandholt, I., Stisen, S., 2006. Evaluating MODIS, MERIS, and VEGETATION vegetation indices using in situ measurements in a semiarid environment. IEEE Trans. Geosci. Rem. Sens. 44, 1774–1786.
Filippa, G., Cremonese, E., Migliavacca, M., Galvagno, M., Forkel, M., Wingate, L., Tomelleri, E., di Cella, U.M., Richardson, A.D., 2016. Phenopix: a R package for image-based vegetation phenology. Agric. Forest Meteorol. 220, 141–150.
Fischer, M.L., Billesbach, D.P., Berry, J.A., Riley, W.J., Torn, M.S., 2007. Spatiotemporal variations in growing season exchanges of CO_2, H_2O, and sensible heat in agricultural fields of the southern great plains. Earth Interact. 11, 1–21.
Flanagan, L.B., Wever, L.A., Carlson, P.J., 2002. Seasonal and interannual variation in carbon dioxide exchange and carbon balance in a northern temperate grassland. Glob. Change Biol. 8, 599–615.
Gamon, J.A., Huemmrich, K.F., Wong, C.Y.S., Ensminger, I., Garrity, S., Hollinger, D.Y., Noormets, A., Peñuelas, J., 2016. A remotely sensed pigment index reveals photosynthetic phenology in evergreen conifers. Proc. Natl. Acad. Sci. U.S.A.
Gillespie, A.R., Kahle, A.B., Walker, R.E., 1987. Color enhancement of highly correlated images. II. Channel ratio and "chromaticity" transformation techniques. Rem. Sens. Environ. 22, 343–365.
Gower, S.T., Vogel, J.G., Norman, J.M., Kucharik, C.J., Steele, S.J., Stow, T.K., 1997. Carbon distribution and aboveground net primary production in aspen, jack pine, and black spruce stands in Saskatchewan and Manitoba, Canada. J. Geophys. Res.: Atmos. 102, 29029–29041.
Havstad, K., Kustas, W., Rango, A., Ritchie, J., Schmugge, T., 2000. Jornada experimental range: a unique arid land location for experiments to validate satellite systems. Rem. Sens. Environ. 74, 13–25.
Heinsch, F., Heilman, J., McInnes, K., Cobos, D., Zuberer, D., Roelke, D., 2004. Carbon dioxide exchange in a high marsh on the Texas gulf coast: effects of freshwater availability. Agric. Forest Meteorol. 125, 159–172.
Hufkens, K., Friedl, M., Sonnentag, O., Braswell, B.H., Milliman, T., Richardson, A.D., 2012. Linking near-surface and satellite remote sensing measurements of deciduous broadleaf forest phenology. Rem. Sens. Environ. 117, 307–321.
Hwang, T., Band, L.E., Miniat, C.F., Song, C., Bolstad, P.V., Vose, J.M., Love, J.P., 2014. Divergent phenological response to hydroclimate variability in forested mountain watersheds. Glob. Change Biol. 20, 2580–2595.
Jin, H., Eklundh, L., 2014. A physically based vegetation index for improved monitoring of plant phenology. Rem. Sens. Environ. 152, 512–525.
Jolly, W.M., Nemani, R., Running, S.W., 2005. A generalized, bioclimatic index to predict foliar phenology in response to climate. Glob. Change Biol. 11, 619–632.
Jönsson, A., Eklundh, L., Hellström, M., Bärring, L., Jönsson", P., 2010. Annual changes in MODIS vegetation indices of Swedish coniferous forests in relation to snow dynamics and tree phenology. Rem. Sens. Environ. 114, 2719–2730.
Keenan, T.F., Darby, B., Felts, E., Sonnentag, O., Friedl, M., Hufkens, K., O' Keefe, J.F., Klosterman, S., Munger, J.W., Toomey, M., Richardson, A.D., 2014. Tracking forest phenology and seasonal physiology using digital repeat photography: a critical assessment. Ecol. Appl 140206175103002.
Klosterman, S.T., Hufkens, K., Gray, J.M., Melaas, E., Sonnentag, O., Lavine, I., Mitchell, L., Norman, R., Friedl, M.A., Richardson, A.D., 2014. Evaluating remote sensing of deciduous forest phenology at multiple spatial scales using PhenoCam imagery. Biogeosciences 11, 4305–4320.
Kosmala, M., Crall, A., Cheng, R., Hufkens, K., Henderson, S., Richardson, A.D., 2016. Season spotter: using citizen science to validate and scale plant phenology from near-surface remote sensing. Rem. Sens. 8, 726.
Liu, L., Liang, L., Schwartz, M.D., Donnelly, A., Wang, Z., Schaaf, C.B., Liu, L., 2015. Evaluating the potential of MODIS satellite data to track temporal dynamics of autumn phenology in a temperate mixed forest. Rem. Sens. Environ. 160, 156–165.
Luo, Y., El-Madany, T., Filippa, G., Ahrens, B., Carrara, A., Gonzalez-Cascon, R., Cremonese, E., Galvagno, M., Hammer, T., Pacheco-Labrador, J., Martín, M.P., Moreno, G., Perez-Priego, O., Reichstein, M., Richardson, A.D., Römermann, C., Migliavacca, M., 2017. Using near-infrared enabled digital repeat photography to track structural and physiological phenology in mediterranean tree-grass ecosystems. Agric. Forest Meteorol (in review).
Magill, A.H., Aber, J.D., Currie, W.S., Nadelhoffer, K.J., Martin, M.E., McDowell, W.H., Melillo, J.M., Steudler, P., 2004. Ecosystem response to 15 years of chronic nitrogen additions at the Harvard Forest LTER, Massachusetts, USA. Forest Ecol. Manag. 196, 7–28 The Harvard Forest (USA) Nitrogen Saturation Experiment: Results from the First 15 Years.
Migliavacca, M., Galvagno, M., Cremonese, E., Rossini, M., Meroni, M., Sonnentag, O., Cogliati, S., Manca, G., Diotri, F., Busetto, L., Cescatti, A., Colombo, R., Fava, F., Morra di Cella, U., Pari, E., Siniscalco, C., Richardson, A.D., 2011. Using digital repeat photography and eddy covariance data to model grassland phenology and photosynthetic CO_2 uptake. Agric. Forest Meteorol. 151, 1325–1337.
Migliavacca, M., Sonnentag, O., Keenan, T.F., Cescatti, A., O'Keefe, J., Richardson, A.D., 2012. On the uncertainty of phenological responses to climate change, and implications for a terrestrial biosphere model. Biogeosciences 9, 2063–2083.
Nagai, S., Saitoh, T.M., Kobayashi, H., Ishihara, M., Suzuki, R., Motohka, T., Nasahara, K.N., Muraoka, H., 2012. In situ examination of the relationship between various vegetation indices and canopy phenology in an evergreen coniferous forest, Japan. Int. J. Rem. Sens. 33, 6202–6214.
Nasahara, K., Nagai, S., 2015. Review: development of an in-situ observation network for terrestrial ecological remote sensing – the phenological eyes network (PEN). Ecol. Res. 30, 211–223.
National Phenology Network, 2017. USA National Phenology Network, Plant and Animal Phenology Data for the United States, 2007–2017. USA-NPN, Tucson, AZ, USA. http://dx.doi.org/10.5066/F78S4N1V. (accessed 14.08.17).
Petach, A.R., Toomey, M., Aubrecht, D.M., Richardson, A.D., 2014. Monitoring vegetation phenology using an infrared-enabled security camera. Agric. Forest Meteorol. 195–196, 143–151.
Richardson, A.D., Braswell, B.H., Hollinger, D.Y., Jenkins, J.P., Ollinger, S.V., 2009. Near-surface remote sensing of spatial and temporal variation in canopy phenology. Ecol. Appl. 19, 1417–1428.
Richardson, A.D., Hufkens, K., Milliman, T., Aubrecht, D.M., Chen, M., Gray, J.M., Johnston, M.R., Keenan, T.F., Klosterman, S.T., Kosmala, M., Melaas, E.K., Friedl,

M.A., Frolking, S., 2017. Tracking vegetation phenology across diverse north American biomes using phenocam imagery. Sci. Data (in review).
Richardson, A.D., Jenkins, J.P., Braswell, B.H., Hollinger, D.Y., Ollinger, S.V., Smith, M.L., 2007. Use of digital webcam images to track spring green-up in a deciduous broadleaf forest. Oecologia 152, 323–334.
Richardson, A.D., Keenan, T.F., Migliavacca, M., Ryu, Y., Sonnentag, O., Toomey, M., 2013. Climate change, phenology, and phenological control of vegetation feedbacks to the climate system. Agri. Forest Meteorol. 169, 156–173.
Rosenzweig, C., Casassa, G., Karoly, D., Imeson, A., Liu, C., Menzel, A., Rawlins, S., Root, T., Seguin, B., Tryjanowski, P., 2007. Assessment of observed changes and responses in natural and managed systems. In: Parry, M.L., Canziani, O.F., Hanson, J.P.P.V.D.L.C. (Eds.), Climate Change 2007: Working Group II: Impacts, Adaptation and Vulnerability. Cambridge University Press, pp. 79–131.
Ryu, Y., Baldocchi, D.D., Verfaillie, J., Ma, S., Falk, M., Ruiz-Mercado, I., Hehn, T., Sonnentag, O., 2010. Testing the performance of a novel spectral reflectance sensor, built with light emitting diodes (LEDS), to monitor ecosystem metabolism, structure and function. Agric. Forest Meteorol. 150, 1597–1606.
Ryu, Y., Lee, G., Jeon, S., Song, Y., Kimm, H., 2014. Monitoring multi-layer canopy spring phenology of temperate deciduous and evergreen forests using low-cost spectral sensors. Rem. Sens. Environ. 149, 227–238.
Sonnentag, O., Hufkens, K., Teshera-Sterne, C., Young, A.M., Friedl, M., Braswell, B.H., Milliman, T., O'Keefe, J., Richardson, A.D., 2012. Digital repeat photography for phenological research in forest ecosystems. Agric. Forest Meteorol. 152, 159–177.
Sonnentag, O., Talbot, J., Chen, J., Roulet, N., 2007. Using direct and indirect measurements of leaf area index to characterize the shrub canopy in an ombrotrophic peatland. Agric. Forest Meteorol. 144, 200–212.
Soudani, K., Hmimina, G., Dufrêne, E., Berveiller, D., Delpierre, N., Ourcival, J.M., Rambal, S., Joffre, R., 2014. Relationships between photochemical reflectance index and light-use efficiency in deciduous and evergreen broadleaf forests. Rem. Sens. Environ. 144, 73–84.
Thomas, C.K., Law, B.E., Irvine, J., Martin, J.G., Pettijohn, J.C., Davis, K.J., 2009. Seasonal hydrology explains interannual and seasonal variation in carbon and water exchange in a semiarid mature ponderosa pine forest in central Oregon. J. Geophys. Res.: Biogeosci. 114, G04006.
Tucker, C.J., 1979. Red and photographic infrared linear combinations for monitoring vegetation. Rem. Sens. Environ. 8, 127–150.
Wingate, L., Ogée, J., Cremonese, E., Filippa, G., Mizunuma, T., Migliavacca, M., Moisy, C., Wilkinson, M., Moureaux, C., Wohlfahrt, G., Hammerle, A., Hörtnagl, L., Gimeno, C., Porcar-Castell, A., Galvagno, M., Nakaji, T., Morison, J., Kolle, O., Knohl, A., Kutsch, W., Kolari, P., Nikinmaa, E., Ibrom, A., Gielen, B., Eugster, W., Balzarolo, M., Papale, D., Klumpp, K., Köstner, B., Grünwald, T., Joffre, R., 2015. Interpreting canopy development and physiology using the EUROPhen camera network at flux sites. Biogeosci. Discuss. 12, 7979–8034.
Zhang, X., Friedl, M., Schaaf, a., Strahler, C.B., Hodges, A.H., Gao, J.C.F., Reed, F., Huete, B.C.A., 2003. Monitoring vegetation phenology using MODIS. Rem. Sens. Environ. 84, 471–475.